ELSEVIER

Journal of Nuclear Materials 276 (2000) 114–122

journal of nuclear materials

www.elsevier.nl/locate/jnucmat

# The microstructure and associated tensile properties of irradiated fcc and bcc metals

M. Victoria[a,*], N. Baluc[a], C. Bailat[a], Y. Dai[b], M.I. Luppo[a,1], R. Schäublin[a], B.N. Singh[c]

[a] *EPFL-CRPP-Fusion Technology Materials, 5232 Villigen PSI (CH), Switzerland*
[b] *Paul Scherrer Institute, 5232 Villigen PSI (CH), Switzerland*
[c] *Department of Materials Research, Risø National Laboratory, 4000 Roskilde (DK), Switzerland*

**Abstract**

The differences and similarities of behaviour between fcc and bcc metals after irradiation have been investigated. For this purpose, fcc Cu, Pd and 304 stainless steel and bcc Fe, Mo and Mo–5% Re were irradiated with either neutrons or 590 MeV protons at temperatures below recovery stage V. It is shown that a dense population of defect clusters (up to $10^{22}$–$10^{24}$ $m^{-3}$) develops, the type of cluster formed depending apparently on the stacking fault energy. In the case of stacking fault tetrahedra formed in Cu, their size is independent of dose, while interstitial loops in stainless steel grow at neutron doses higher than 1 dpa. The defect microstructure is found to be independent of the recoil energy spectra in this temperature region, but shows a very strong dependence on the type of crystalline structure. The results of tensile testing indicate the presence of radiation hardening, starting at very low doses as an upper yield point develops followed by a (serrated) yield region. The main deformation mode observed is dislocation channeling. The hardening is modelled in terms of the initial dislocation locking by the irradiation-induced defects followed by the dispersed hardening induced by the global distribution of clusters in the matrix. 

## 1. Introduction

The defect microstructure induced by irradiation in metals has been extensively studied since the early observations of Silcox and Hirsch in neutron irradiated copper, nearly 40 years ago [1]. Since then, improvements of both the electron microscope and the observation techniques have greatly advanced our knowledge of the field and it is by now well established that in the displacement cascade regime a high density of defect clusters forms, typically in the configuration of stacking fault tetrahedra (SFT) or small interstitial loops, resulting from the quenching and evolution of the cascade. Two subjects are of interest for the present study. First, a number of differences between dissimilar types of crystal structure have been demonstrated by previous observations. There are clear indications that the majority of defects in fcc Cu produced in the low temperature regime (0.1–0.2 $T_m$, where $T_m$ is the melting temperature) are SFTs [2,3] as compared to loops and small 'black dots' in bcc Fe [4] and Mo [5]. Furthermore, Jenkins et al. [6] have shown, in ion irradiation experiments, that there is apparently also a difference in the rate of accumulation of the defect clusters, bcc Fe showing a smaller rate of accumulation with dose than fcc Ni and Cu. The argument has been further developed in a more recent work by Singh and Evans [7], who have argued that the rate of accumulation and its temperature dependence are different for fcc and bcc metals, in particular regarding the region where swelling will occur. Moreover, present computer simulations of the cascade and defect microstructure evolution show results in the same direction: the size and fraction of self-interstitial atoms (SIA) clusters are larger in Cu than in Fe [8]. The vacancies on the other hand, are in Cu mostly in the form of clusters, while they do not cluster in Fe [9].

* Corresponding author. Fax: +41-56 310 4529.
*E-mail address:* victoria@psi.ch (M. Victoria).
[1] On leave from the Department of Metallurgy, Comision Nacional de Energia Atomica, Argentina.

0022-3115/00/$ - see front matter 
PII: S0022-3115(99)00203-2

It is important then to systematise this view by performing irradiation experiments in fcc and bcc materials of comparable quality.

The second problem of interest is that of the effects of the recoil energy spectra. The use of irradiations with high energy protons is here of particular interest, since a very hard recoil spectrum (medium energy ~1–2 MeV in Cu) is produced by the irradiation with this type of particle. Previous results [2,3] have shown no differences between the defect microstructures in Cu after irradiation with either neutrons or high energy protons in the temperature regime of interest in the present study.

The experiments presented here compare the effects of irradiation with fission neutrons or high energy protons on the microstructure and resulting tensile properties between fcc Cu and Pd on one side and bcc Fe, Mo and Mo–5%Re on the other.

## 2. Experimental procedure

The materials used in these experiments are (i) fcc Cu (99.99%) and Pd (99.999%) single crystals, oriented along a $\langle 1\,1\,0\rangle$ axis, (ii)Polycrystalline Fe (99.95%) with a grain size of 50 μm, (iii) Mo and Mo–5%Re single crystals and polycrystals and (iv) type 304 stainless steel, with a composition in wt% of 18.32Cr/10.42Ni/1.16Mn/0.029Co/0.13Si/0.021P/0.011S/0.013C/0.0005B/0.027N.

Flat microtensile specimens, with a 5.5 mm gauge length and 300 μm thickness, were produced from all materials. This geometry has been shown to reproduce bulk results for material with a maximum grain size of 30–50 μm [10].

All neutron irradiations, except for the stainless steel, took place in the reactor at Risø National Laboratory (DK), which has a flux of $2.5\times10^{17}$ nm$^{-2}$ s$^{-1}$ ($E > 1$ MeV) which results in a damage rate of $5\times10^{-8}$ s$^{-1}$ in Cu. The recoil spectrum is typical of fission, with a mean energy of 30 keV. The stainless steel was irradiated in the Barseback reactor in Sweden where the fast neutron flux is between $1.5\times10^{17}$ and $7.6\times10^{17}$ nm$^{-2}$ s$^{-1}$.

Proton irradiations took place in the PIREX facility which uses the 590 MeV proton beam of the accelerator at the Paul Scherrer Institute in Switzerland [11]. Protons of this energy have a range of several centimetres in Cu or Fe. The displacement damage distribution is therefore in the bulk of the target and is produced by the recoiling nucleus resultant from a spallation nuclear reaction. This results in a PKA spectrum with mean energies of the order of 1–2 MeV. The spallation reaction produces also He at a rate of ~100 appm per dpa in the metals irradiated in this study. Proton currents of 10 μA were mostly used in the present investigation, which results in a damage rate of $5\times10^{-7}$ dpa s$^{-1}$.

The irradiation temperatures were in the range of 300–320 K, which correspond to 0.15–0.2 $T_m$ for Cu, Pd and Fe, where $T_m$ is their melting point and they are well below the recovery stage V in these materials. The stainless steel, on the other hand, was irradiated at 520 K, which is the temperature of reference for light water reactors. Doses attained were between $10^{-3}$ and 1 dpa.

Electron microscopy observations were performed either with the JEOL 2010 at PSI or the JEOL 2000FX at Risø National Laboratory, both operating at 200 kV. Defect microstructure observations were performed using bright/dark field and weak beam techniques, using different ng(mg) conditions as indicated in each case. Defect number densities and size distributions were obtained from three or four regions of the same specimen with 100–400 defects (Cu, Pd, stainless steels) or 50–100 defects (Fe).

## 3. Results and discussion

### 3.1. The irradiation-induced defect microstructure

The defect microstructures resulting from proton irradiation at 300 K in Cu at two different doses and a comparable one in Pd are shown in Fig. 1, together with the resulting size distributions. The first point to note is that the mean defect cluster size in Cu remains constant with a dose at ~2 nm. Second, although the size distribution is similar in Pd at comparable doses, the fractions of the different types of defect are reversed: a majority of the defect clusters observed in Cu are stacking fault tetrahedra, while small loops form the major fraction of defects in Pd.

A comparison between the microstructures after neutron and proton irradiation is shown in Fig. 2(a) for polycrystalline pure Fe and in Fig. 3(a) for polycrystalline Mo–5%Re irradiated with protons and in Figs. 2(b) and 3(b) for the same Fe and for single crystal Mo–5%Re irradiated with neutrons. The microstructure consists in both cases of small loops, with comparable size distributions and analogous mean sizes. The character of the loops was not analysed in every case, but they are most probably of interstitial type.

The same outcome has been obtained in technical alloys. Results from both proton and neutron irradiation in 304L stainless steel are shown in Fig. 4. A distribution of small loops is observed after both types of irradiation, but while a well-defined loop size distribution with a mean size of 3.14 nm is found after the relatively low dose proton irradiation (Fig. 4(a)), a somewhat irregular and relatively broad size distribution is found after 1.5 dpa neutron irradiation, Fig. 4(b), with half maximum values of 5.7 and 12 nm.

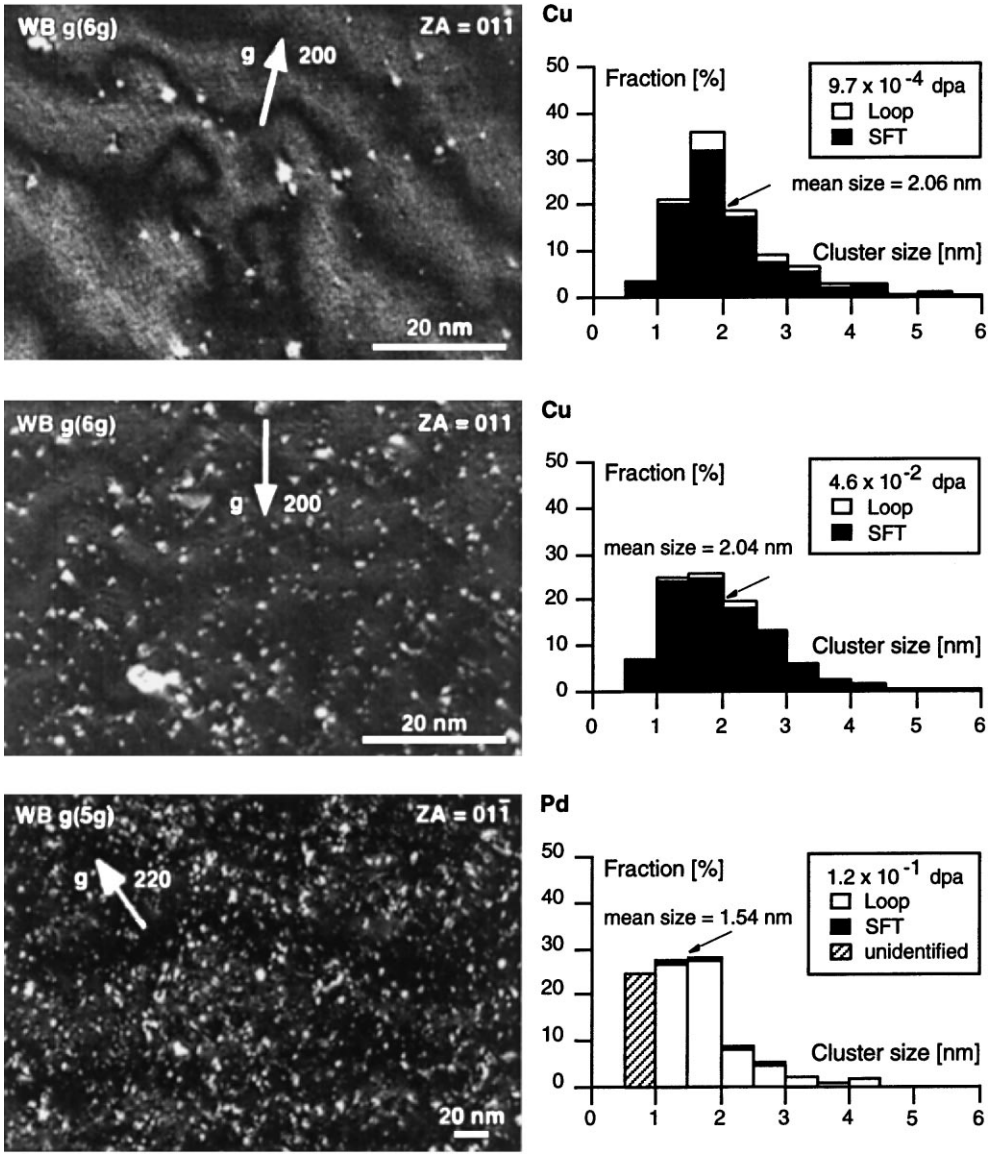


Fig. 1. Different defect microstructures observed after proton irradiation at $T_{irr} = 320$ K and their defect size distribution: (i) Cu irradiated to $9.7 \times 10^{-4}$ and $4.6 \times 10^{-2}$ dpa, (ii) Pd irradiated to $1.2 \times 10^{-1}$ dpa.

In terms of the type of defects, these observations indicate that in low stacking fault energy Cu, the majority of defects observed are SFTs, while, as the SFE increases in Pd or in bcc metals, small dislocation loops are the main result of the irradiation with either protons or neutrons. The higher the SFE the more difficult it will be to form SFTs. Corresponding values of SFE are 45 mJ $m^{-2}$ in Cu compared to 180 mJ $m^{-2}$ in Pd [12]. In this context, the austenitic stainless steel, which has a low SFE ($\sim$40 mJ $m^{-2}$), is atypical in that the main population of defect clusters are loops and not SFTs. It indicates also that the SFE is not the only controlling factor defining the type of cluster that will form in a given material.

In the case where the preponderant defect clusters are SFTs, it can be expected that the mean size of the defect microstructure does not increase with dose, since there is very little vacancy mobility in the temperature region where the present experiments have been performed and the cascades where the defects originate are well separated in this low dose regime. On the other hand, when the main defects observed are interstitial loops, they will grow with dose by the accumulation of the mobile SIA

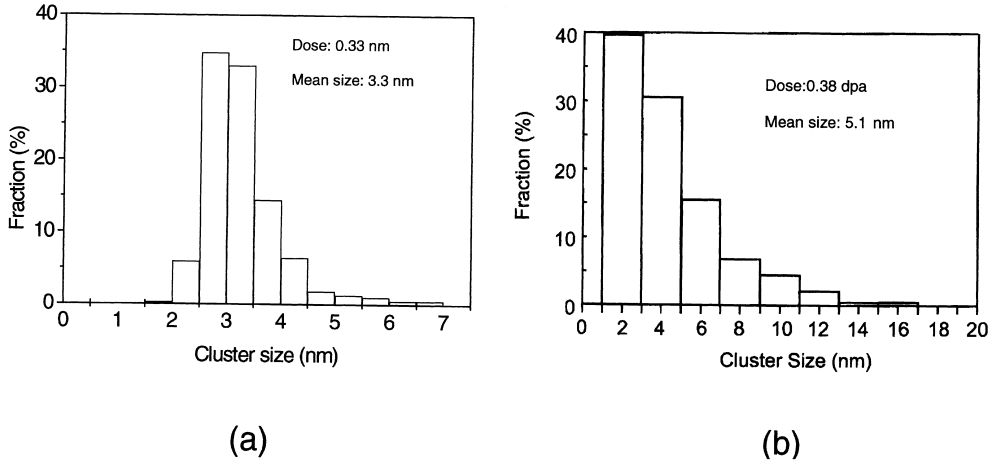


Fig. 2. Size distributions of clusters in polycrystalline pure Fe: (a) irradiated with protons; (b) same material after neutron irradiation at $T_{irr} = 320$ K.

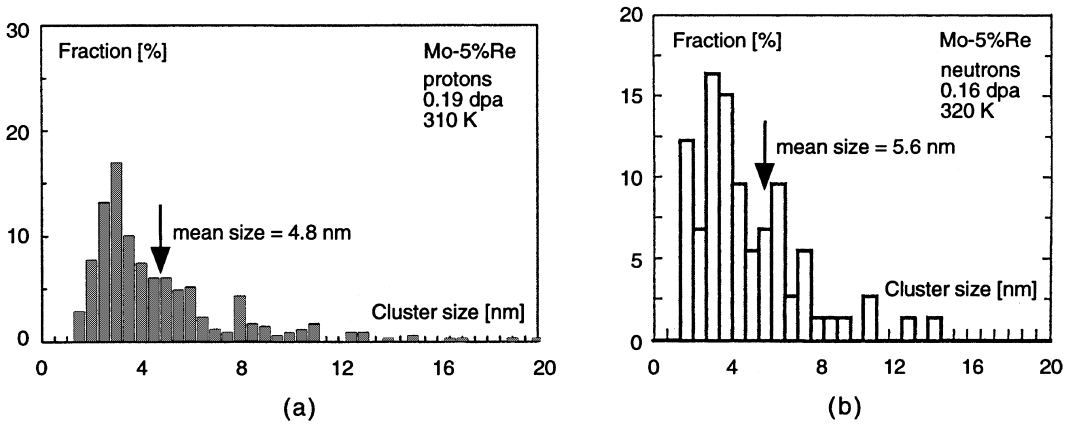


Fig. 3. Size distributions of: (a) polycrystalline pure Mo–5%Re, irradiated with protons; (b) neutron-irradiated Mo–5%Re single crystal.

clusters and the growth from an initial population of smaller size will give rise to a broad size distribution at sufficiently higher doses.

The number density of defects is plotted as a function of dose in Fig. 5. The slope of the log/log plot is 0.83–0.9, so almost a linear dependence is found for Cu, Pd or Fe. The slope is identical whether irradiated with protons or neutrons, and the saturation of cluster density is evident in the case of Cu at a dose of $\sim 10^{-2}$ dpa. But in Fe, three orders of magnitude higher doses are needed to attain the same defect density. It should be noted here, however, that in the case of Fe, it still remains uncertain as to at what dose and cluster density levels the cluster density may come to saturate. High dose experiments would be very useful in answering this uncertainty.

The dose dependence of the number density is generally taken as an indication that the majority of the defect clusters actually originate from the cascade condensation, as it would be difficult to explain such linear relation with a mechanism of homogeneous nucleation and growth, but a reliable conclusion can only be drawn for the SFTs in Cu.

The main difference observed between fcc and bcc metals in terms of the microstructure induced by the irradiation is a large difference in the rate of accumulation, which is structure and not type of defect dependent: both in fcc Pd and Fe the defects observed are loops, but Fe needs one thousand times more dose to reach the same defect density. The reasons for this difference are not entirely clear at this point, but computer simulations of cascade evolution indicate that while

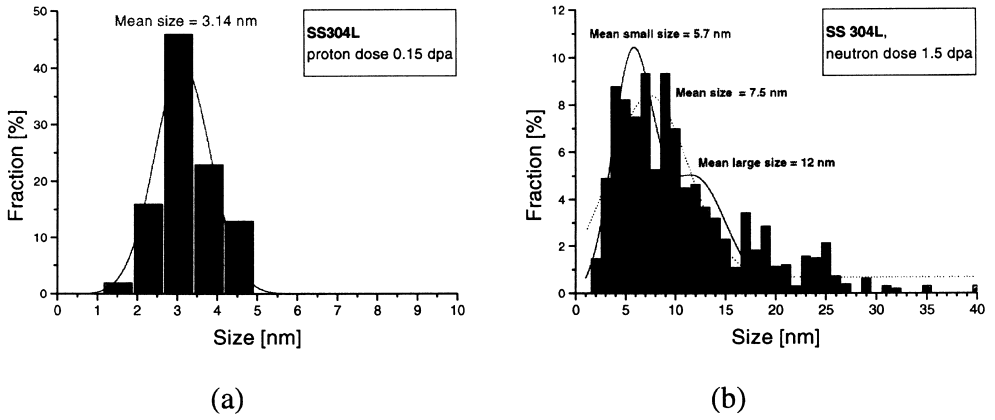


Fig. 4. Loop size distributions in 304L stainless steel: (a) after proton irradiation; (b) after neutron irradiation at $T_{irr} = 550$ K.

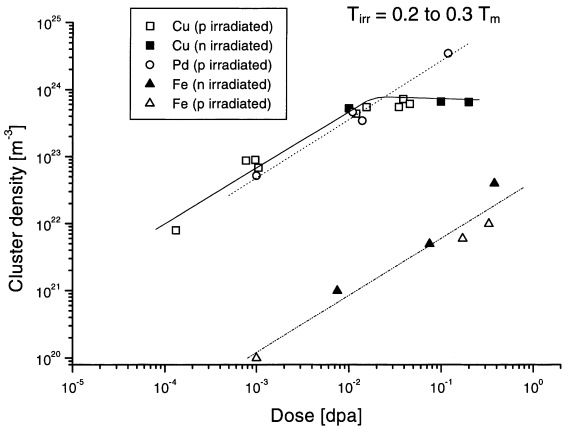


Fig. 5. Defect number density in Cu, Pd and Fe after irradiation with neutrons or protons.

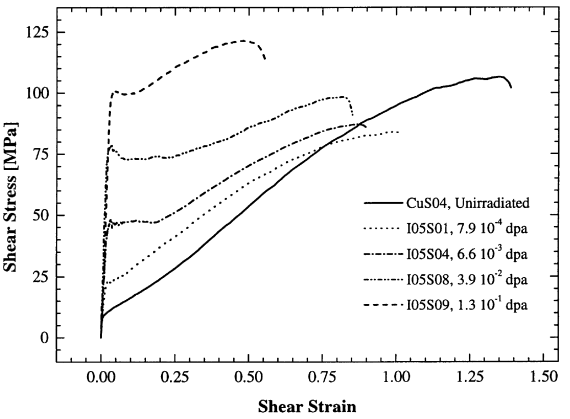


Fig. 6. The shear stress–shear strain curves of Cu single crystals, proton irradiated to different doses at ambient temperature. Displacement doses (in dpa) are indicated on the stress–strain curves.

stable SFTs result from large cascades (for PKAs ~30–50 keV) in Cu [13], interstitial loops resulting from the cascade quenching in Fe are much smaller and highly mobile [8,9,14].

### 3.2. Tensile properties and deformation modes

The tensile curves obtained from proton-irradiated Cu single crystals at several doses are shown in Fig. 6, together with the corresponding curve for the unirradiated material. Hardening is present even at very low doses, together with the progressive appearance of an upper yield point and the development of a serrated yield region at practically constant average shear stress. The hardening increases with dose and has not saturated yet at the highest dose observed, 0.2 dpa, at which point it is almost one order of magnitude higher compared to the unirradiated critical shear stress value. The total shear strain before fracture also decreases with dose. The deformation is highly localised. Surface observations [15], indicate the formation of localised slip bands, which form and develop, as the shear strain increases, in several points along the gauge length. This development takes place at practically average constant stress, during the outgrowth of what we have called the yield region. It is only when the gauge length has been fully covered by slip bands that strain hardening starts to take place.

A comparable behaviour is found for polycrystals, deformed after either proton or neutron irradiation. Fig. 7 shows the behaviour of polycrystalline Fe. While at very low doses (~$10^{-3}$ dpa) only an increase in the yield strength is observed, at doses of the order of $10^{-2}$ dpa a further increase in the yield strength is accompanied by almost the disappearance of the work hardening in the tensile behaviour and a loss of ductility.

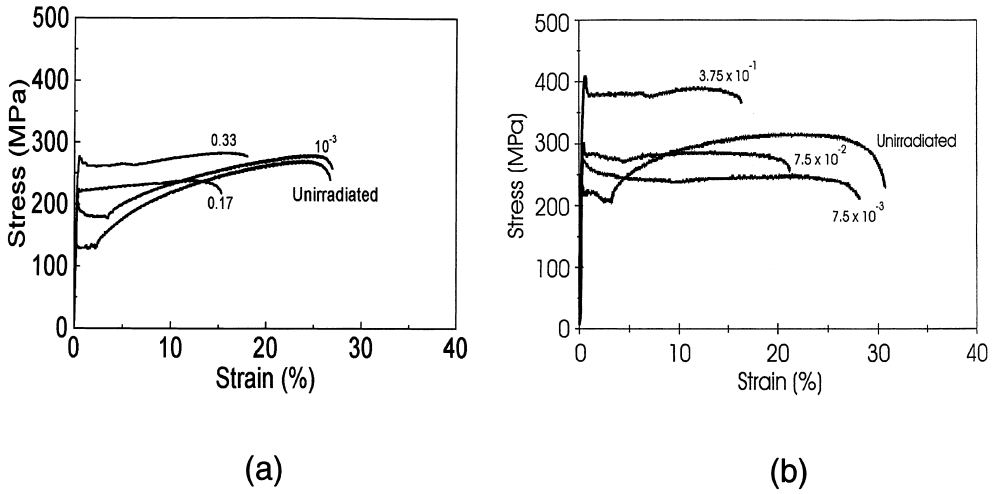


Fig. 7. Tensile deformation of polycrystalline Fe: (a) proton irradiated; (b) neutron irradiated.

There are two contributions to the increase of strength of the irradiated material. On the one hand, the original dislocation structure present in the crystal will be pinned down by the defects produced during irradiation. A clear example in neutron-irradiated Mo single crystal is shown in Fig. 8, where dislocations are locked by small clusters with a very small separation. Notice also that there is a distribution of loops in the rest of the crystal matrix, but at a lower density and larger spacing. Trinkaus et al. [16] have lately reviewed the conditions for this dislocation decoration and arrived at the conclusion that the direct clustering of SIAs or vacancies in a region near the dislocation cannot be due to three-dimensional diffusion and agglomeration of single SIAs, but rather that the decoration is produced by the accumulation of one-dimensionally migrating glissile loops, that were produced originally in the cascades. MD simulations [14,17,18] have actually demonstrated this one-dimensional motion. The clusters remain in a metastable state near to the dislocation and can only be absorbed by it after a thermally activated [16,19,20] or elastic force field-induced [21] change in Burgers vector direction.

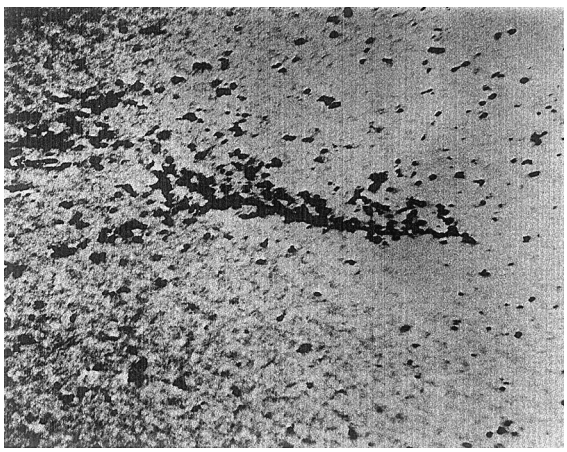

Fig. 8. Dislocation locking in neutron-irradiated Mo single crystal at 320 K.

The dislocation pinning will give rise to a source hardening described in [19]: the dislocations have initially to free themselves from the clusters to be able to glide in their slip plane. A model for stress needed in the unpinning process has been formulated by the authors mentioned above [19,20]. They model a straight row of sessile loops of diameter $d$ and Burgers vector $b$, spaced at a distance $l$ along the dislocation line at a stand-off distance $y$. The dislocation itself has a Burger vector $b$ and is contained in an isotropic media of shear modulus $\mu$ and Poisson ratio $v$. The applied shear stress $\tau_{UY}$ needed to unlock the dislocation from the loop atmosphere, which will correspond to the upper yield point is given by

$$\tau_{UY} = 0.1\mu\ [b/l]\ (d/y)^2.$$

Using the values for Cu ($\mu = 55$ GPa, $b = 0.256$ nm) and taking the value of $\tau_{UY} = 50$ MPa obtained from Fig. 6 for the I05S04 Cu crystal irradiated with protons to $6.6 \times 10^{-3}$ dpa, at which dose the upper yield point is first clearly observable, the relation $ly^2 = 118$ nm$^3$ is obtained when the measured average value of $d = 2.05$ nm is used. The stand-off distance $y$ is unknown and atomistic calculations are needed to get its proper value, but following the discussion in [19] it can be estimated to be of the order of the loop size $d$. The distance $l$ must then be of the order of $10b$ in order to account for the upper yield point. The values are not only reasonable,

but the value of $l$ compares well with that of TEM observations.

The second contribution will come from the unlocked source dislocation that will then multiply and interact with the distribution of defect clusters present in the matrix of the crystal which are separated at a much larger distance: for the crystal taken as an example in the above discussion the mean distance in the matrix $L = (Nd)^{-1/2} \sim 280$ nm, a factor of about one hundred times larger than the value for dislocation locking. It has been shown [3,15] that the hardening by this defect structure is well represented by the dispersed obstacle model [22], where the increase of strength, beyond the upper yield point, compared to the unirradiated state, is given by

$$\Delta\tau = \alpha\mu b(Nd)^{1/2},$$

where $\alpha$ is a factor that accounts for the strength of the obstacle. It was found [3] that in the irradiated Cu single crystals there is a linear relation between the measured values of $\Delta\tau$ and $(Nd)^{1/2}$ with a resultant value of $\alpha = 0.1 - 0.2$, which describes soft obstacles. It should be pointed out that these measurements were performed in the yield region. Beyond it, as it is further discussed in Section 3.3, the contribution from dislocation–dislocation interaction to the work hardening is the main component of the flow stress. Furthermore, for higher dose levels, where only a yield region at approximate constant stress level (see Fig. 7) is observed, $\Delta\tau$ reflects the resistance to dislocation motion in the channels.

The main mode of deformation observed associated with the localised strain behaviour is the formation of dislocation channels, of which examples in Pd and Fe are shown in Fig. 9. The moving dislocation sweeps the defects in the slip plane, leaving the slip plane depleted of them in its wake. Succeeding dislocations in the same plane will find fewer obstacles on their way, provoking a strong localisation of the deformation in channel-like regions of the crystal.

A second deformation mode has been found to be active in austenitic stainless steels. Fig. 10(b) shows the localisation of strain by deformation twinning in 304L stainless steel, neutron irradiated at 550 K but deformed at room temperature. The twins are once again free of defects. As the deformation temperature is raised and equals that of irradiation, the deformation mode reverts to that of dislocation channeling, Fig. 10(a).

It is important to note here a significant consequence of such localised modes of deformation. While in single crystals the associated strain will be relaxed at the surface, grain boundaries in polycrystals might not be able to do so and result in local microcracking. Cracking at grain boundaries as a consequence of dislocation channeling or deformation twinning of the irradiated material has now been observed in Fe [23], austenitic stainless steels [24] and ferritic-martensitic steels [25].

### 3.3. The activation volume

The activation volume is a measure of the volume of interaction of the dislocation with the obstacle and provides a good indication on the type of operating mechanism in this interaction. The method used here is that of successive relaxations at different stress levels in the tensile curve. The cross-head of the tensile machine is stopped and the stress $\Delta\tau_{rel}$ is measured. The apparent

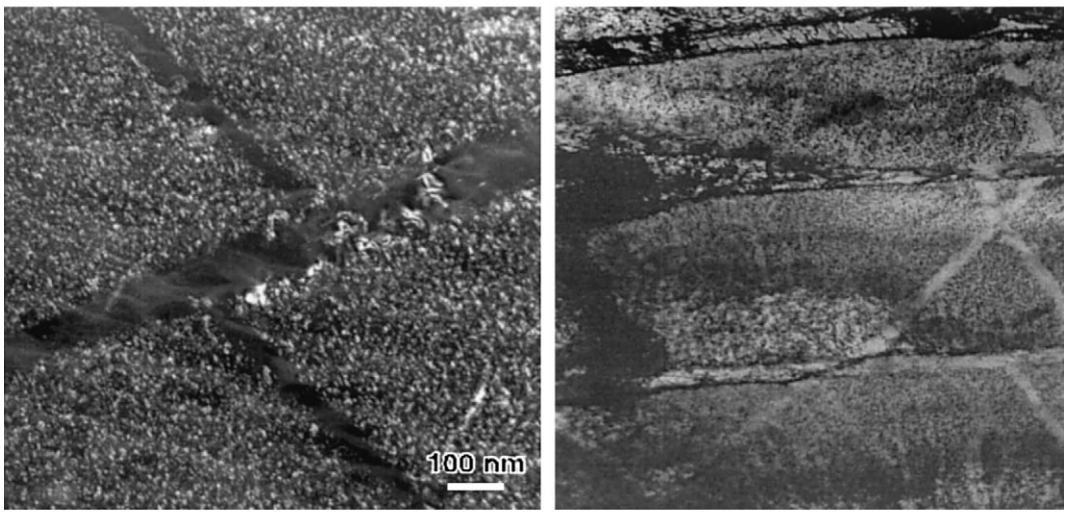


Fig. 9. Dislocation channeling in Pd single crystals irradiated with protons (a) and in polycrystalline Fe irradiated with neutrons (b).

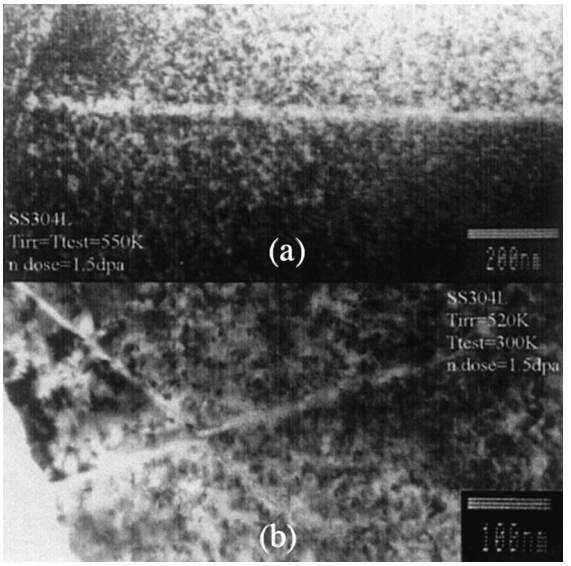


Fig. 10. Deformation modes in neutron-irradiated 304L stainless steel: (a) dislocation channeling in the steel tested at 550 K; (b) deformation twins in the test at room temperature.

activation volume $V_a$ for a single relaxation is given in this case by [26]

$$\Delta\tau_{rel} = kT/V_a \ln(1 + t/c),$$

where $t$ is the relaxation time, $T$ the test temperature, $k$ the Boltzmann constant and $c$ is an adjustable time constant. As $V_a$ depends on the hardening of the sample and the stiffness of the testing machine, a correction is introduced by performing successive relaxations in order to obtain the effective activation volume $V_{eff}$ [27].

Measurements in the Cu single crystals are plotted in Fig. 11 as a function of the shear strain. In the unirradiated case, the activation volume decreases rapidly as the strain increases, and tends asymptotically to a value of $150b^3$, where $b$ is the module of the Burgers vector.

The initial values of $V_{eff}$ measured for irradiated specimens correspond to the dislocation–defect cluster interaction, as exemplified in crystal I05S04 irradiated to $6.6\times10^{-3}$, where a value of $540b^3$ obtained in the yield region compares well with that of $485b^3$ obtained from the simple geometrical calculation of a dislocation of length $L = 280$ nm moving over an obstacle of diameter $d = 2.05$ nm. It should be noted that these values correspond to the region where dislocation channeling is the deformation mode. As the deformation proceeds and the density of obstacles decreases through the interaction with dislocations, the mean length $L$ increases, to the point that interaction with other (forest) dislocations becomes the dominant mechanism.

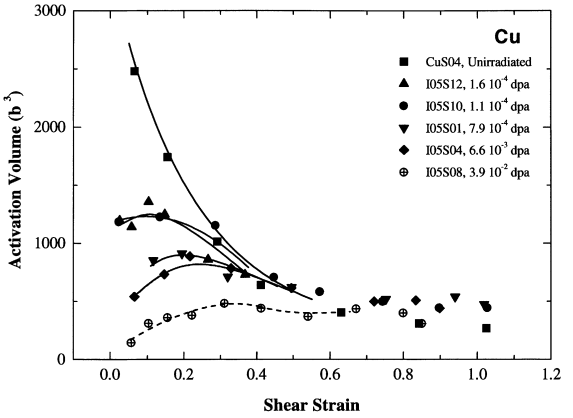


Fig. 11. Effective activation volumes for dislocation–defect interaction in Cu single crystals , deformed at 300 K.

## 4. Conclusions

From the results of irradiations in fcc Cu, Pd and 304L austenitic stainless steel and bcc Fe, Mo and Mo–5%Re, with either fission neutrons or 590 MeV protons, it can be concluded that:

- A high density ($10^{22}$–$10^{24}$ $m^{-3}$) of defect clusters is found. The majority of clusters are SFTs in Cu while in Pd and Fe they are interstitial loops, showing that for low stacking fault energy metals (Cu), SFTs form, while loops are the main component of the microstructure for high SFE metals Pd and Fe. Austenitic stainless steels are an exception to this trend in that the SFE is low but loops are formed.
- The cluster defect distributions have constant mean size with increasing dose at low doses. The mean size of the loop distributions increases with dose beyond a dose of ~1 dpa, forming a bimodal size distribution.
- Three orders of magnitude higher dose are needed to produce the same defect density in Fe as compared to Cu.
- No effect of the recoil energy spectra has been found in the temperature range of the present irradiations.
- There is a rapid increase of the yield stress with dose, with the progressive appearance of an upper yield point followed by a yield region at approximately constant (lower) stress. In single crystals, work hardening starts at the end of the yield region.
- The main deformation mode observed is dislocation channeling, which strongly localises the strain. In 304 stainless steel, deformation twins play a similar role.
- These deformation characteristics can be well associated with the defect cluster microstructure through modelling that explains the yield point in terms of dislocation decoration and locking by defect clusters, followed by the interaction of the gliding dislocation with the cluster density in the matrix of the crystal.

These mechanisms are further evidenced by the behaviour of the effective activation volume.

## Acknowledgements

The authors would like to acknowledge the financial assistance of the Swiss National Research Fund and the European Fusion Technology Program. The assistance of ABB Nuclear Sweden in providing irradiated stainless steel specimens is also recognised. One of the authors (M.I.L.) wishes to express her gratitude to the Fundacion Antorchas for the travel funds received.

## References

[1] J. Silcox, P.B. Hirsch, Philos. Mag. 4 (1959) 1356.
[2] B.N. Singh, S.J. Zinkle, J. Nucl. Mater. 206 (1993) 212.
[3] Y. Dai, M. Victoria, Mat. Res. Soc. Symp. Proc. 439 (1996) 319.
[4] B.N. Singh, A. Horsewell, P. Toft, J. Nucl. Mater. 271–272 (1999) 97.
[5] B.N. Singh, J.H. Evans, A. Horsewell, P. Toft, G.V. Müller, J. Nucl. Mater. 258–263 (1998) 865.
[6] M.L. Jenkins, M.A. Kirk, W.J. Pythian, J. Nucl. Mater. 205 (1993) 212.
[7] B.N. Singh, J.H. Evans, J. Nucl. Mater. 226 (1995) 277.
[8] W.J. Pythian, R.E. Stoller, A.J.E. Foreman, A.F. Calder, D.J. Bacon, J. Nucl. Mater. 223 (1995) 245.
[9] M.J. Caturla, N. Soneda, E. Alonso, B. Wirth, T. Diaz de la Rubia, J.M. Perlado, these Proceedings, p. 13.
[10] P. Spätig, R. Schaublin, S. Gyger, M. Victoria, J. Nucl. Mater. 253–258 (1998) 1345.
[11] P. Marmy, M. Daum, D. Gavillet, S. Green, W.V. Green, F. Hegedus, S. Proennecke, U. Rohrer, U. Stiefel, M. Victoria, Nucl. Instrum. and Meth. B 47 (1990) 212.
[12] N. Baluc, Y. Dai, M. Victoria, Mater. Res. Soc. Symp. Proc. 540 (1999).
[13] K. Nordlung, F. Gao, Appl. Phys. Lett., submitted.
[14] Y.N. Osetsky, D.J. Bacon, A. Serra, B.N. Singh, S.I. Golubov, these Proceedings, p. 65.
[15] Y. Dai, Ph.D. thesis No 1388, École Polytechnique Fédérale de Lausanne, 1995.
[16] H. Trinkaus, B.N. Singh, A.J.E. Foreman, J. Nucl. Mater. 249 (1997) 91.
[17] N. Soneda, T. Diaz de la Rubia, Philos. Mag. 78 (1998) 995.
[18] B.D. Wirth, G.R. Odette, D. Maroudas, G.E. Lucas, these Proceedings, p. 33.
[19] B.N. Singh, A.J.E. Foreman, H. Trinkaus, J. Nucl. Mater. 249 (1997) 103.
[20] H. Trinkaus, B.N. Singh, A.J.E. Foreman, J. Nucl. Mater. 251 (1997) 172.
[21] N.M. Ghoniem, B.N. Singh, L.Z. Sun, T. Diaz de la Rubia, these Proceedings, p. 166.
[22] J.L. Fleischer, J. Appl. Phys. 33 (1962) 835.
[23] Y. Chen, P. Spätig, M. Victoria, J. Nucl. Mater. 271&272 (1999) 128.
[24] C. Bailat, F. Gröschel, M. Victoria, these Proceedings, p. 283.
[25] Y. Dai, F. Carsughi, W.F. Sommer, G.S. Bauer, H. Ullmaier, these Proceedings, p. 289.
[26] F. Guiu, P.L. Pratt, Phys. Stat. Sol. 34 (1969) 9.
[27] L.P. Kubin, Philos. Mag. 30 (1974) 705.